Strong Coulomb scattering effects on low frequency noise in monolayer WS2 field-effect transistors

Min-Kyu Joo, Yoojoo Yun, Seokjoon Yun, Young Hee Lee, and Dongseok Suh

Citation: Applied Physics Letters **109**, 153102 (2016); doi: 10.1063/1.4964467
View online: http://dx.doi.org/10.1063/1.4964467
View Table of Contents: http://scitation.aip.org/content/aip/journal/apl/109/15?ver=pdfcov
Published by the AIP Publishing

Strong Coulomb scattering effects on low frequency noise in monolayer WS_2 field-effect transistors

Min-Kyu Joo,[1,2,a)] Yoojoo Yun,[2,a)] Seokjoon Yun,[1,2] Young Hee Lee,[1,2] and Dongseok Suh[2,b)]
[1]*Center for Integrated Nanostructure Physics (CINAP), Institute for Basic Science (IBS), Suwon 16419, South Korea*
[2]*Department of Energy Science, Sungkyunkwan University, Suwon 16419, South Korea*

(Received 7 July 2016; accepted 26 September 2016; published online 10 October 2016)

When atomically thin semiconducting transition metal dichalcogenides are used as a channel material, they are inevitably exposed to supporting substrates. This situation can lead to masking of intrinsic properties by undesired extrinsic doping and/or additional conductance fluctuations from the largely distributed Coulomb impurities at the interface between the channel and the substrate. Here, we report low-frequency noise characteristics in monolayer WS_2 field-effect transistors on silicon/silicon-oxide substrate. To mitigate the effect of extrinsic low-frequency noise sources, a nitrogen annealing was carried out to provide better interface quality and to suppress the channel access resistance. The carrier number fluctuation and the correlated mobility fluctuation (CNF-CMF) model was better than the sole CNF one to explain our low-frequency noise data, because of the strong Coulomb scattering effect on the effective mobility caused by carrier trapping/detrapping at oxide traps. The temperature-dependent field-effect mobility in the four-probe configuration and the Coulomb scattering parameters are presented to support this strong Coulomb scattering effect on carrier transport in monolayer WS_2 field-effect transistor. *Published by AIP Publishing.*
[http://dx.doi.org/10.1063/1.4964467]

Atomically thin two-dimensional (2D) layered materials such as graphene, hexagonal boron nitride (BN), and transition metal dichalcogenides (TMDs) opened up new research fields of 2D electronic systems.[1–5] In particular, various semiconducting TMDs show a desirable bandgap of 1–2 eV, which can be further controlled by the material's thickness varying from bulk- to monolayer-state.[1,6–9] Among various combinations of TMDs, a monolayer WS_2 has recently gained great interests because of its high thermal stability, high on-/off-current ratio with in-plane field-effect mobility, low subthreshold swing, and large thickness-dependent bandgap energy.[10–14] Due to those beneficial features, a monolayer WS_2 can be one of good candidate materials for highly performing, low-power-consumption electronic and optoelectronic devices especially useful in a variety of sensing applications.

The atomically thin nature of layered TMDs such as monolayer MoS_2 or WS_2 makes their electrical transport properties sensitively influenced by the underlying substrate unlike the case of bulk materials. It is intuitively clear that the intimate contact between the channel TMD materials and the underlying substrate can induce various charge scattering processes degrading the intrinsic properties of TMDs. Experimentally, the low-frequency (LF) $1/f$ noise analysis is a powerful and nondestructive tool to study the Coulomb charge-fluctuation mechanism, surface trap distribution, and reliability in 2D surface-dominant electronic systems.[15,16] For example, the role of hexagonal BN for carrier transport on graphene[17,18] and the metal work function effects on the electron and hole carrier fluctuations in multilayer WSe_2 field-effect transistors (FETs)[19] were investigated using the LF noise characterization. Besides, a contribution of the channel and that of the contacts to the total LF noise characteristics were also studied for MoS_2 FETs in addition to the thickness effect.[20,21] Furthermore, there are several reports concerning the Coulomb scattering effect on various TMD materials, especially on MoS_2.[10,20–27]

However, no experimental study on LF noise characteristics of monolayer WS_2 FETs has been performed yet, except that there is one report concerning an emission current noise analysis of multilayer WS_2 nanosheets.[28] In this letter, we study the strong Coulomb scattering effect on LF noise characteristics of monolayer WS_2 FET in the insulating regime. The carrier number fluctuation and correlated mobility fluctuation (CNF-CMF) model can fit the experimental data well, which determines the surface trap density and Coulomb scattering coefficient (α_{SC}), respectively. Furthermore, the temperature dependence of the field-effect mobility (μ_{FE}) and that of α_{SC} are analyzed to support the importance of Coulomb scattering mechanism in this monolayer 2D device revealed by the LF noise analysis.

Monolayer WS_2 flakes synthesized using a chemical vapor deposition (CVD) technique were transferred onto silicon substrate with 300-nm-thick SiO_2 dielectrics. After the identification of proper triangular-shaped WS_2 flakes using an optical microscope, a selective electron-beam lithography patterning and Cr/Au (2 nm/50 nm) bimetal deposition followed by the lift-off process were carried out to make the source (S) and drain (D) electrodes. To have a clean surface and suppress the channel access resistance, the WS_2 FETs were annealed at low vacuum (under 10^{-2} Torr) and high

[a)]M.-K. Joo and Y. Yun contributed equally to this work.
[b)]Author to whom correspondence should be addressed. Electronic mail: energy.suh@skku.edu

temperature (150 °C) for 5 h in a nitrogen (N_2) gas with 100 sccm condition. The thickness (~0.75 nm) of monolayer WS_2 was confirmed by an atomic force microscope (AFM) as displayed in Figure 1(a) and the length (L), and width (W) of the WS_2 channel were measured using the commercial optical microscope (Axio imager 2, CARL ZEISS).

Figure 1(b) displays the device schematic and the representative sample image of the WS_2 FET. The structure of the monolayer WS_2 on SiO_2 was characterized by Raman spectroscopy (XperRam 200, Nano Base) with a 100 μW excitation laser at wavelength $\lambda_{exc} = 532$ nm shown in Figure 1(c). Using a multipeak Lorentzian fitting process, the dominant Raman peaks corresponding to different vibration modes were identified; A_{1g} at 417.3 cm^{-1} for out-of-plane optical phonon mode, E^1_{2g} at 355 cm^{-1} for in-plane optical phonon mode, and 2LA(M) at 350.2 cm^{-1} for the second-order longitudinal acoustic phonon mode. The frequency difference between A_{1g} and E^1_{2g} was 62.3 cm^{-1}, which is almost consistent with the reported Raman peak for monolayer WS_2.[10,12,29] The remaining peak of 520 cm^{-1} is measured from Si substrate.

Figure 2(a) displays the representative drain-to-source current (I_{DS}) curves as a function of back gate bias (V_{BG}) at a fixed drain voltage ($V_D = 1.0$ V) before and after the N_2 annealing process, whose channel length (L) and width (W) are 2 μm and 27 μm, respectively. Because this annealing process can remove undesired adsorbents on the surface of WS_2 such as water and oxygen molecules, a clear enhancement of the electrical performance could be observed in terms of the increased on-current value, the high on-/off-current ratio (~10^5), the downshifted turn-on voltage (~15 V), and the sufficiently suppressed hysteresis phenomena. In addition to the channel properties, the electrical contact barrier height also reduced significantly so that the device could be regarded to have an ohmic-like contact at room temperature, as can be seen in the $I_{DS}-V_D$ output characteristics in Figure 2(b). As a result, the calculated maximum field-effect mobility μ_{FE} ($=Lg_m/(WC_{OX}V_D)$, where C_{OX} is the gate capacitance per unit area and $g_m = \partial I_{DS}/\partial V_{BG}$ is the transconductance) was enhanced from ~10^{-3} to ~1 $cm^2\ V^{-1}\ s^{-1}$, and the interface trap density obtained from the simplified subthreshold swing model[25,30–33] ($SS \approx \ln(10)k_BT(1 + qD_{IT}/C_{OX})/q$, where q, T, k_B, and D_{IT} denote electron charge, absolute temperature, Boltzmann constant, and interface trap density) was decreased by a factor of two on average, as shown in Figures 2(c) and 2(d).

It is worth noting that the absolute value of μ_{FE} in our CVD-grown monolayer WS_2 FET is much smaller than the previously reported value μ_{FE} (~80 $cm^2\ V^{-1}\ s^{-1}$) of the mechanically exfoliated sample,[10] even though the μ_{FE} in our sample was enhanced by a factor of 10^3 after the N_2 annealing process. This low μ_{FE} indicates that our sample shows the charge conduction in the insulating regime of WS_2, which might be ascribed to the substantial defects such as sulfur vacancies and grain boundaries as shown in Figure 1(a) owing to the CVD process.[34,35] Moreover, the high degree of interface trap density (10^{11}–10^{13} $cm^{-2}eV^{-1}$) from SiO_2 substrate can also be another reason for the mobility degradation.[25]

Figure 3(a) displays the exemplary current power spectrum density (S_I) curves of the monolayer WS_2 FET for the LF noise characteristics. They were measured in a dark metal shielding box under a high vacuum condition with V_{BG} varying from 10 to 52.5 V at $V_D = 1.0$ V. All data curves show the typical $1/f$ dependence from 5 Hz to 5 kHz. Concerning the current fluctuation mechanism, I_{DS} normalized S_I (NSI) curves as a function of I_{DS} at a fixed frequency ($f = 12$ Hz) are displayed in Figure 3(b) for the high mobility sample and in Figure 3(c) for the low mobility one, respectively. Among many fabricated devices, a few samples having a relatively high μ_{FE} showed a good correlation with the NSI in the CNF[16,36] (i.e., $\text{NSI} = S_{VFB}(g_m/I_{DS})^2$, where S_{VFB} is the flat-band voltage power spectral density) as shown in Figure 3(b). This observation indicates that the dominant $1/f$ LF noise mechanism is related to the free carrier trapping/detrapping processes with oxide traps, leading to variations in the flat-band voltage ($S_{VFB} = q^2k_BTN_{ST}/(LWC_{OX}{}^2f)$). Note that the Hooge mobility fluctuation (HMF) model,[16,37] where the NSI is simply inversely proportional to I_{DS} (red lines in Figures 3(b) and 3(c)) will not be considered in the following LF noise analysis because of too much of discrepancy.

Most of the samples, however, were well described by the CNF-CMF[16,38] ($\text{NSI} = S_{VFB}(1 + \alpha_{SC}\mu_{eff}C_{OX}I_{DS}/g_m)^2(g_m/I_{DS})^2$ instead of the CNF, as shown in Figure 3(c). In fact, the main scattering mechanism of the $1/f$ flicker noise is the variation in the number of carriers. The only difference is that the CNF-CMF model takes the additional noise caused by the occupancy of the oxide traps into account, which in turn is correlated with fluctuations in the carrier number and the surface mobility simultaneously. When the atomic thickness of a monolayer and the diminishing screening length of TMD materials are considered, the CNF-CMF model could be a more accurate model to interpret the $1/f$ noise data in the 2D

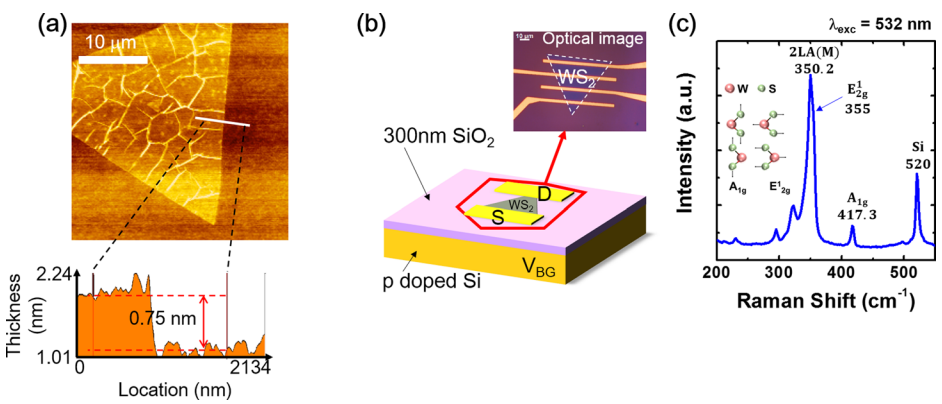

FIG. 1. (a) Representative AFM image of a monolayer WS_2 flake. The bottom thickness profile corresponds to the thin white line in the top AFM image. (b) Device schematic of the monolayer WS_2 FET. The right top inset displays a representative optical microscope image of the fabricated sample. (c) Raman spectrum of the WS_2 monolayer flake on SiO_2.

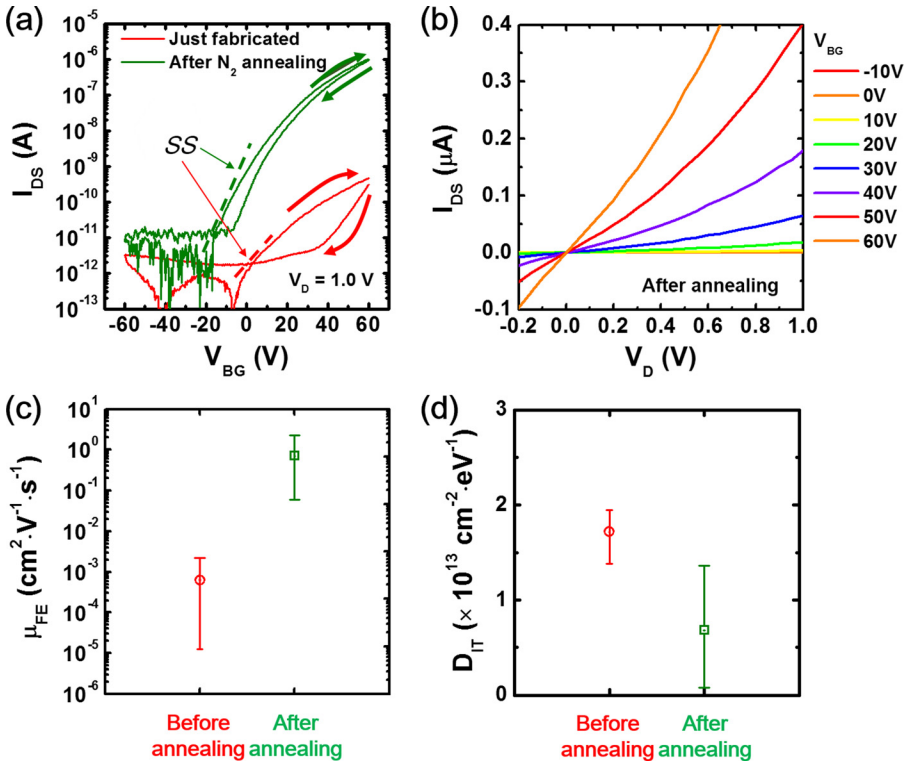

FIG. 2. (a) Representative $I_{DS}-V_{BG}$ transfer curves measured at $V_D = 1.0$ V before (red) and after (green) N_2 annealing. (b) $I_{DS}-V_D$ output characteristics for various values of V_{BG} after N_2 annealing. Annealing effect on (c) μ_{FE} and (d) the interface trap density (D_{IT}) of the monolayer WS_2 FETs.

system, because the free carriers in the 2D channel are sufficiently close to the largely distributed Coulomb impurities in the channel or in the underlying dielectrics to have interaction with each other.

Figure 3(c) gives the clear discrepancy between the CNF and the CNF-CMF models from the subthreshold to high accumulation regimes. In the conventional CNF-CMF model, the empirically determined α_{SC} has been regarded as a constant, which is actually valid only in the case of bulk Si metal–oxide–semiconductor FETs ($\alpha_{SC} \approx 10^4$ V s C^{-1} and $\approx 10^5$ V s C^{-1} for electrons and holes, respectively).[16,27,38] Here we consider α_{SC} ($=q^{-1}\mu_{C0}{}^{-1}n_{2D}{}^{-\gamma}$, where μ_{C0} is constant and γ is an exponent) as a function of the 2D-accumulated carrier density (n_{2D}) because of the diminishing screening effects from reduced dimensionality.[39] This argument is supported by the recent report concerning remote Coulomb scattering effect in fully depleted silicon-on-insulator (FD-SOI) devices with an ultrathin silicon film (7 nm), where the V_{BG} dependence of α_{SC} and the carrier centroid distance from the high-k top-gate dielectric are present.[40,41]

When the above α_{SC} effect is taken into account, the n_{2D} dependence of α_{SC} ($\mu_{C0} \sim 3.9 \times 10^{-9}$ cm^2 V^{-1} s^{-1} and $\gamma \sim 0.9$) is obtained as shown in Figure 3(d). This indicates that the interfacial Coulomb scattering effect in 2D TMD materials is stronger than that in bulk-silicon-based transistors because of the different Coulomb scattering screening lengths. As n_{2D} increases, α_{SC} quickly decreases in the subthreshold regime, but it seems to be eventually saturated at a certain density in the large accumulation regime. Although this anomalous strong Coulomb scattering effect on LF noise characteristics might be partially caused by the undesired external noise sources from the channel access resistance or the electrical barrier height, the main noise sources can be the largely distributed Coulomb impurities inside WS_2 and/or SiO_2 substrate.

To study the strong Coulomb scattering effect on carrier transport and LF noise characteristics in more detail, we carried out the temperature-dependent static and LF noise measurements in a commercial low-temperature measurement system (Lake Shore CRX-VF cryogenic probe station). To exclude the external contact resistance effect, we employed

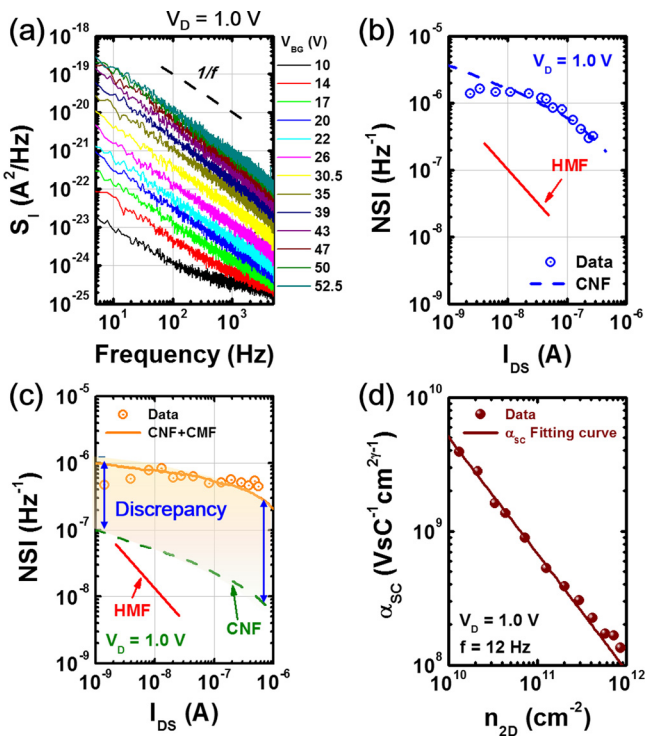

FIG. 3. (a) Frequency (f) dependence of the drain current power spectrum density (S_I) curves as a function of V_{BG} at $V_D = 1.0$ V. (b)–(c) Variation of the NSIs for WS_2 transistors, estimated from the relatively high-μ_{FE} (b) and low-μ_{FE} (c) values at $f = 12$ Hz and fitted with the CNF, HMF, and CNF-CMF models. (d) Plot of α_{SC} as a function of n_{2D} for the monolayer WS_2 FET.

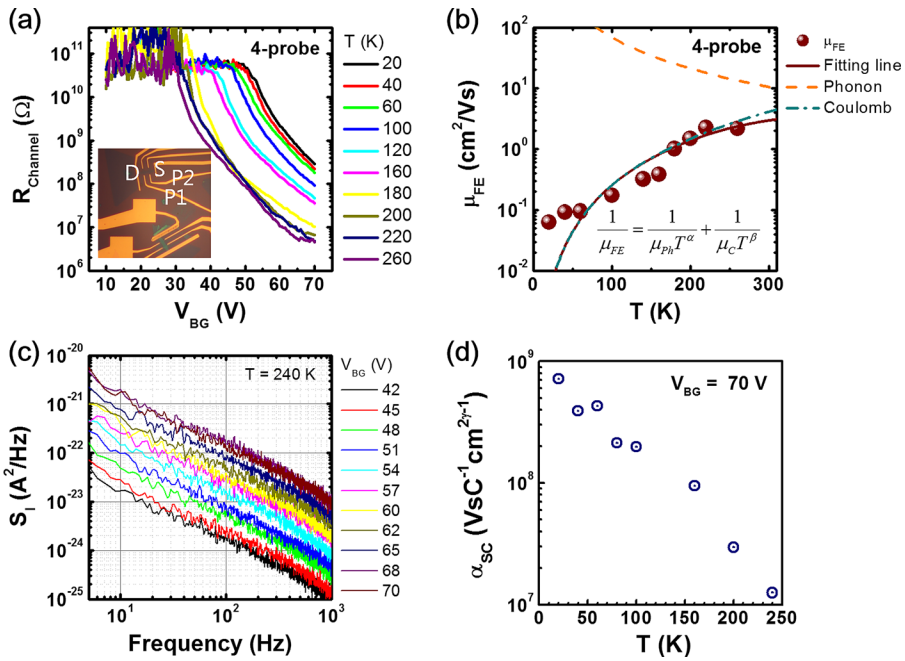

FIG. 4. (a) R_{channel} as a function of V_{BG} at various temperatures and (b) μ_{FE} as a function of temperature for the monolayer WS_2 FET in the four-probe configuration. The calculated total μ_{FE} curve (brown line) from the simplified Matthiessen rule, μ_C (dark green long dashed and dotted line) and μ_{Ph} (orange long-dashed line) are displayed together (The channel length L and width W in the inset of (a) are 3 μm and 15 μm, respectively). (c) Plot of the S_I curves for various V_{BG} at $T = 240$ K. (d) Temperature dependence of α_{SC} at $V_{BG} = 70$ V.

the four-probe measurement configuration as shown in the inset of Figure 4(a), where a reactive ion etching process using an SF_6 plasma was applied to define the active channel area of WS_2 and two voltage probes (P1, P2) were added. Temperature-dependent channel resistance (R_{channel}) curves as a function of V_{BG} are displayed in Figure 4(a) at different temperatures. Because of the largely distributed Coulomb impurities at the interface, the carrier transport was mainly limited to the insulating regime.

For the systematic investigation of the carrier scattering mechanism for the monolayer WS_2 FET, the μ_{FE} measured in the four-probe configuration is plotted as a function of temperature in Figure 4(b). To identify the contribution of various scattering mechanisms such as Coulomb impurity scattering and/or phonon scattering, the simplified Matthiessen rule $\mu_{FE} = 1/(\mu_{Ph}T^{\alpha}) + 1/(\mu_C T^{\beta})$ was used to fit the data curve, where μ_C, μ_{Ph}, α, and β denote the Coulomb-limited mobility, optical-phonon-limited mobility, and the corresponding exponents, respectively. It can be clearly seen that the strong Coulomb scattering effect dominates the overall carrier transport in the observed temperature range, leading to a large carrier number fluctuation.[22,26,42,43]

To verify this experimentally, we measured the temperature-dependent LF noise characteristics down to 20 K in a dark metal vacuum chamber. Figure 4(c) displays the S_I curves as a function of V_{BG} from 42 to 70 V at $T = 240$ K, showing a typical $1/f$ dependence. After fitting the obtained NSI data to the CNF-CMF model at $f = 20$ Hz as previously demonstrated, we determined the temperature dependence of α_{SC} at $V_{BG} = 70$ V as shown in Figure 4(d). The obtained α_{SC} decreases sharply as temperature increases because of the thermionic excitation effect, but the degree of amplitude is still high. Hence, the role of α_{SC} in the LF noise analysis cannot be ignored in 2D WS_2 FETs in the insulating regime. The estimated surface trap density ranges from $\sim 10^{13}$ to $\sim 10^{14}\,\text{eV}^{-1}\,\text{cm}^{-2}$ depending on the temperature, which is equivalent to $2.6 \times 10^{10}\,\text{cm}^{-2} \leq D_{IT} \times k_B T \leq 5.2 \times 10^{11}\,\text{cm}^{-2}$. Such results are comparable to that of CVD grown-MoS_2 device case,[35] and almost identical to the range of interface trap density estimated from the subthreshold swing.

In summary, we studied the electrical transport and the LF noise characteristics in the CVD-synthesized monolayer WS_2 FETs on silicon/silicon-oxide substrate. The carrier number fluctuation is found to govern the LF noise characteristics, and the large discrepancy between the CNF model and the CNF-CMF model could be explained by the variable α_{SC} with respect to the 2D-accumulated carrier density, where the diminished screening effects are caused by reduced dimensionality. Moreover, from the temperature dependence of μ_{FE} and α_{SC}, the anomalous strong Coulomb scattering effect on carrier mobility and LF noise characteristics is attributed to the largely distributed Coulomb impurities inside the channel WS_2 and the underlying SiO_2. Such a strong Coulomb scattering effect is expected to be reduced by the adoption of a hexagonal BN thin film or that of high-dielectric-constant passivation layer to enhance the electrical properties of this 2D device.[10,17,18,39]

This work was supported by the Institute for Basic Science (IBS-R011-D1) (Y.H.L.), Republic of Korea and also supported by the Basic Science Research (NRF-2013R1A1A1076063) (D.S.) through the National Research Foundation of Korea, funded by the Ministry of Science, ICT and Future Planning, Republic of Korea.

[1]D. Jariwala, V. K. Sangwan, L. J. Lauhon, T. J. Marks, and M. C. Hersam, ACS Nano **8**, 1102 (2014).
[2]K. S. Novoselov, D. Jiang, F. Schedin, T. J. Booth, V. V. Khotkevich, S. V. Morozov, and A. K. Geim, Proc. Natl. Acad. Sci. U.S.A. **102**, 10451 (2005).
[3]S. Z. Butler, S. M. Hollen, L. Cao, Y. Cui, J. A. Gupta, H. R. Gutiérrez, T. F. Heinz, S. S. Hong, J. Huang, A. F. Ismach, E. Johnston-Halperin, M. Kuno, V. V. Plashnitsa, R. D. Robinson, R. S. Ruoff, S. Salahuddin, J. Shan, L. Shi, M. G. Spencer, M. Terrones, W. Windl, and J. E. Goldberger, ACS Nano **7**, 2898 (2013).
[4]K. S. Novoselov, V. I. Falko, L. Colombo, P. R. Gellert, M. G. Schwab, and K. Kim, Nature **490**, 192 (2012).

[5]C. R. Dean, A. F. Young, I. Meric, C. Lee, L. Wang, S. Sorgenfrei, K. Watanabe, T. Taniguchi, P. Kim, K. L. Shepard, and J. Hone, Nat. Nanotechnol. **5**, 722 (2010).
[6]A. H. Castro Neto, F. Guinea, N. M. R. Peres, K. S. Novoselov, and A. K. Geim, Rev. Mod. Phys. **81**, 109 (2009).
[7]J. A. Wilson and A. D. Yoffe, Adv. Phys. **18**, 193 (1969).
[8]Q. H. Wang, K. Kalantar-Zadeh, A. Kis, J. N. Coleman, and M. S. Strano, Nat. Nanotechnol. **7**, 699 (2012).
[9]W. Zhao, Z. Ghorannevis, L. Chu, M. Toh, C. Kloc, P.-H. Tan, and G. Eda, ACS Nano **7**, 791 (2013).
[10]M. W. Iqbal, M. Z. Iqbal, M. F. Khan, M. A. Shehzad, Y. Seo, J. H. Park, C. Hwang, and J. Eom, Sci. Rep. **5**, 10699 (2015).
[11]K.-K. Kam, Ph.D. thesis, Iowa State University, Ames, Iowa, 1982.
[12]D. Ovchinnikov, A. Allain, Y.-S. Huang, D. Dumcenco, and A. Kis, ACS Nano **8**, 8174 (2014).
[13]F. Withers, T. H. Bointon, D. C. Hudson, M. F. Craciun, and S. Russo, Sci. Rep. **4**, 4967 (2014).
[14]Y. Cui, R. Xin, Z. Yu, Y. Pan, Z.-Y. Ong, X. Wei, J. Wang, H. Nan, Z. Ni, Y. Wu, T. Chen, Y. Shi, B. Wang, G. Zhang, Y.-W. Zhang, and X. Wang, Adv. Mater. **27**, 5230 (2015).
[15]G. Ghibaudo and T. Boutchacha, Microelectron. Reliab. **42**, 573 (2002).
[16]M. von Haartman and M. Östling, *Low-Frequency Noise in Advanced MOS Devices* (Springer, Berlin, 2007).
[17]X. Li, X. Lu, T. Li, W. Yang, J. Fang, G. Zhang, and Y. Wu, ACS Nano **9**, 11382 (2015).
[18]M. A. Stolyarov, G. Liu, S. L. Rumyantsev, M. Shur, and A. A. Balandin, Appl. Phys. Lett. **107**, 023106 (2015).
[19]S.-P. Ko, J. M. Shin, Y. J. Kim, H.-K. Jang, J. E. Jin, M. Shin, Y. K. Kim, and G.-T. Kim, Appl. Phys. Lett. **107**, 242102 (2015).
[20]J. Renteria, R. Samnakay, S. L. Rumyantsev, C. Jiang, P. Goli, M. S. Shur, and A. A. Balandin, Appl. Phys. Lett. **104**, 153104 (2014).
[21]S. L. Rumyantsev, C. Jiang, R. Samnakay, M. S. Shur, and A. A. Balandin, IEEE Electron Device Lett. **36**, 517 (2015).
[22]B. W. H. Baugher, H. O. H. Churchill, Y. Yang, and P. Jarillo-Herrero, Nano Lett. **13**, 4212 (2013).
[23]V. K. Sangwan, H. N. Arnold, D. Jariwala, T. J. Marks, L. J. Lauhon, and M. C. Hersam, Nano Lett. **13**, 4351 (2013).
[24]Z. Yu, Y. Pan, Y. Shen, Z. Wang, Z.-Y. Ong, T. Xu, R. Xin, L. Pan, B. Wang, L. Sun, J. Wang, G. Zhang, Y. W. Zhang, Y. Shi, and X. Wang, Nat. Commun. **5**, 5290 (2014).
[25]M. Y. Chan, K. Komatsu, S.-L. Li, Y. Xu, P. Darmawan, H. Kuramochi, S. Nakaharai, A. Aparecido-Ferreira, K. Watanabe, T. Taniguchi, and K. Tsukagoshi, Nanoscale **5**, 9572 (2013).
[26]B. Radisavljevic and A. Kis, Nat. Mater. **12**, 815 (2013).
[27]S. Deepak, A. Matin, M. Abhishek, B. S. Pankaj, A. G. Birdwell, N. Sina, M. A. Pulickel, L. Jun, D. Madan, L. Qiliang, and V. D. Albert, Nanotechnology **25**, 155702 (2014).
[28]S. R. Suryawanshi, P. S. Kolhe, C. S. Rout, D. J. Late, and M. A. More, Ultramicroscopy **149**, 51 (2015).
[29]A. Berkdemir, H. R. Gutiérrez, A. R. Botello-Méndez, N. Perea-López, A. L. Elías, C.-I. Chia, B. Wang, V. H. Crespi, F. López-Urías, and J.-C. Charlier, Sci. Rep. **3**, 1755 (2013).
[30]S. M. Sze and K. K. Ng, *Physics of Semiconductor Devices* (John Wiley & Sons, 2006).
[31]X. Liu, K.-W. Ang, W. Yu, J. He, X. Feng, Q. Liu, H. Jiang, T. Dan, J. Wen, Y. Lu, W. Liu, P. Cao, S. Han, J. Wu, W. Liu, X. Wang, D. Zhu, and Z. He, Sci. Rep. **6**, 24920 (2016).
[32]H. Fang, S. Chuang, T. C. Chang, K. Takei, T. Takahashi, and A. Javey, Nano Lett. **12**, 3788 (2012).
[33]S. Kim, P. D. Carpenter, R. K. Jean, H. Chen, C. Zhou, S. Ju, and D. B. Janes, ACS Nano **6**, 7352 (2012).
[34]P. K. Chow, R. B. Jacobs-Gedrim, J. Gao, T.-M. Lu, B. Yu, H. Terrones, and N. Koratkar, ACS Nano **9**, 1520 (2015).
[35]H. Y. Jeong, S. Y. Lee, T. H. Ly, G. H. Han, H. Kim, H. Nam, Z. Jiong, B. G. Shin, S. J. Yun, J. Kim, U. J. Kim, S. Hwang, and Y. H. Lee, ACS Nano **10**, 770 (2016).
[36]A. McWhorter, M.I.T. Lincoln Laboratory Report No. 80, May 1955.
[37]F. N. Hooge, Physica B+C **83**, 14 (1976).
[38]G. Ghibaudo, O. Roux, C. Nguyen-Duc, F. Balestra, and J. Brini, Phys. Status Solidi A **124**, 571 (1991).
[39]H. Ji, M.-K. Joo, Y. Yun, J.-H. Park, G. Lee, B. H. Moon, H. Yi, D. Suh, and S. C. Lim, ACS Appl. Mater. Interfaces **8**, 19092 (2016).
[40]C. G. Theodorou, E. G. Ioannidis, S. Haendler, N. Planes, F. Arnaud, F. Andrieu, T. Poiroux, O. Faynot, J. Jomaah, C. A. Dimitriadis, and G. Ghibaudo, in *Proceedings of the IEEE 2012 International Semiconductor Conference Dresden-Grenoble (2012 ISCDG)*, Grenoble, France, 24–26 September 2012, pp. 223–226.
[41]C. G. Theodorou, E. G. Ioannidis, S. Haendler, N. Planes, F. Arnaud, J. Jomaah, C. A. Dimitriadis, and G. Ghibaudo, in *Proceedings of the 42nd European Solid State Device Research Conference (ESSDERC 2012)*, Bordeaux, France, 18–20 September 2012, pp. 334–337.
[42]S. Das, H.-Y. Chen, A. V. Penumatcha, and J. Appenzeller, Nano Lett. **13**, 100 (2013).
[43]D. Jariwala, V. K. Sangwan, D. J. Late, J. E. Johns, V. P. Dravid, T. J. Marks, L. J. Lauhon, and M. C. Hersam, Appl. Phys. Lett. **102**, 173107 (2013).